PCCP

Accepted Manuscript




ROYAL SOCIETY OF CHEMISTRY

www.rsc.org/pccp

PHYSICAL CHEMISTRY CHEMICAL PHYSICS

ARTICLE

# Photoluminescence properties and energy transfer in color tunable $MgZn_2(PO_4)_2$: $Ce^{3+}$, $Tb^{3+}$ phosphors

Received 00th January 20xx,
Accepted 00th January 20xx

DOI: 10.1039/x0xx00000x

www.rsc.org/

Mengjiao Xu,[a] Luxiang Wang,[a] Dianzeng Jia*[a] and Hongyang Zhao [a]

A series of $Ce^{3+}$/$Tb^{3+}$ co-doped $MgZn_2(PO_4)_2$ phosphors have been synthesized by co-precipitation method. Their structure, morphology, photoluminescence properties, decay lifetime, thermal stability and luminous efficiency were investigated. The possible energy transfer mechanism was proposed based on the experimental results and detailed luminescence spectra and decay curves of the phosphors. The critical distance between $Ce^{3+}$ and $Tb^{3+}$ ion was calculated by both concentration quenching method and spectral overlap method. The energy transfer mechanism from $Ce^{3+}$ to $Tb^{3+}$ ion was determined to be dipole-quadrupole interaction, and the energy transfer efficiency was 85%. By utilizing the principle of energy transfer and appropriate tuning of $Ce^{3+}$/$Tb^{3+}$ contents, the emission color of the obtained phosphors can be tuned from blue to green light. The $MgZn_2(PO_4)_2$: $Ce^{3+}$, $Tb^{3+}$ phosphor is proved to be promising UV-convertible material capable of green light emitting in UV-LEDs due to its excellent thermal stability and luminescence properties.

## 1. Introduction

Recently, considerable research efforts have been directed towards the development of the rare earth ($RE^{3+}$) doped functional materials since they can be used as highly efficient phosphors, catalysts and optics materials by virtue of their unique optical, electronic, and chemical properties[1-5]. Terbium ($Tb^{3+}$) ion is well known as a green emitting activator owing to its predominant $^5D_4$-$^7F_5$ transition peak around 544 nm [6-8]. Moreover, the characteristic sharp emissions of $Tb^{3+}$ originating from intra-configurational 4f-4f transitions are almost independent of the host lattice since the 4f orbital is shielded by the filled $5s^2$ and $5p^6$ orbitals, which leads to the excellent reproduction quality of the optical properties of the phosphor. However, the intensities of $Tb^{3+}$ absorption peaks in the ultraviolet (UV) region are very weak and the widths are quite narrow due to the strictly forbidden 4f-4f transition. In order to intensify the absorption of $Tb^{3+}$ in the UV region, one of the strategies is to use $Ce^{3+}$ as a sensitizer because it has a strong excitation band originating from allowed 4f-5d transitions, which could efficiently absorb the UV light and transfer the excitation energy to $Tb^{3+}$. This kind of energy transfer has been reported in a number of $Ce^{3+}$, $Tb^{3+}$ co-doped phosphors, including silicates, borates, aluminates, phosphates, molybdates, etc. For example, $BaY_2Si_3O_{10}$: $Ce^{3+}$, $Tb^{3+}$, $BaCaBO_3F$: $Ce^{3+}$, $Tb^{3+}$, $Sr_3AlO_4F$: $Ce^{3+}$, $Tb^{3+}$, $LaPO_4$: $Ce^{3+}$, $Tb^{3+}$, $NaLa(MoO_4)_2$: $Ce^{3+}$,$Tb^{3+}$ [9-13].

As an important family of luminescent materials, orthophosphates have great potential applications in the novel luminescent materials due to their low synthesizing temperature, environment benignity, as well as high chemical and physical stability. Among them, zinc orthophosphates have three crystal modifications, labelled as α, β and γ forms.1): α-$Zn_3(PO_4)_2$ with tetrahedrally coordinated cations; 2): β-$Zn_3(PO_4)_2$ with five-coordinated cations and six-coordinated cations; 3): γ-$Zn_3(PO_4)_2$ does not exist, but must be stabilized with respect to α-$Zn_3(PO_4)_2$ by replacing part of the zinc ions with some of the divalent cations, such as Mg, Mn or Cd[14-19]. Such γ phases have been investigated owing to their potential application as luminescence materials. According to literature it is possible to substitute one-third of zinc ions by magnesium ions in γ-$Zn_3(PO_4)_2$, and the doped is stable at room temperature. $Mg^{2+}$ is the only stabilizing ion fulfilling the condition in the stable γ phase. $MgZn_2(PO_4)_2$ has a monoclinic unit cell and contains four five-coordinated cations and two six-coordinated cations[19]. However, to the best of our knowledge, few reports have been made regarding the microstructural and luminescent characteristics of $MgZn_2(PO_4)_2$ co-doped with $Ce^{3+}$, $Tb^{3+}$ ions.

In this work, $Ce^{3+}$ and $Tb^{3+}$ doped $MgZn_2(PO_4)_2$ were synthesized by the co-precipitation method. The crystal structure, morphology, luminescence properties, decay lifetimes, thermal stability and optimal doping concentrations of $Ce^{3+}$ and $Tb^{3+}$ were investigated in order to search for new phosphor materials for potential applications. Colors from blue to green were achieved by solely varying the doping concentration of the $Tb^{3+}$ ions. The energy

[a] *Key Laboratory of Material and Technology for Clean Energy, Ministry of Education, Key Laboratory of Advanced Functional Materials, Autonomous Region, Institute of Applied Chemistry, Xinjiang University, Urumqi 830046, Xinjiang, PR China*

† Corresponding author: *E-mail: jdz@xju.edu.cn/jdz0991@gmail.com Tel.: +86-991-8583083; Fax: +86-991-8588883

Electronic Supplementary Information (ESI) available: [details of any supplementary information available should be included here]. See DOI: 10.1039/x0xx00000x

transfer mechanism of $Ce^{3+}$-$Tb^{3+}$ has been discussed in detail and the critical distance between the doped ions has been calculated by both the concentration quenching method and the spectral overlap method.

## 2. Experimental

### 2.1 Synthesis

$MgZn_2(PO_4)_2$: $xCe^{3+}$, $yTb^{3+}$ ($0 \leqslant x \leqslant 0.12$, $0 \leqslant y \leqslant 0.04$) were synthesized by co-precipitation method. According to the particular stoichiometric ratio, $Mg(NO_3)_2$ (AR), $Zn(NO_3)_2$ (AR), $Ce(NO_3)_3{\cdot}6H_2O$ (AR) and $Tb(NO_3)_3{\cdot}6H_2O$ (AR) were weighed and dissolved in distilled water. $(NH_4)_2HPO_4$ (AR) solution was added dropwise to the nitrate aqueous solution at room temperature. After stirring for several hours, a large quantity of white precipitate was obtained. The precipitate was filtered, washed with distilled water, and then dried at 100 °C for 8 hours to yield the precursor. The ground precursor was sintered in a quartz tube reactor at 850 °C for 2 h in reducing atmosphere (5%$H_2$-95%$N_2$), followed by cooling down naturally to room temperature. Finally, the white products were ground for further characterizations and tests.

### 2.2 Characterization

Powder X-ray diffraction (XRD) measurements were performed on a Bruker D8 Advance Diffraction diffractometer in the 2θ range from 10° to 80° with Cu K*α* radiation (λ= 0.15405 nm) at 40 kV, 40 mA. The morphology and size of the as-synthesized phosphors were studied by scanning electron microscopy (SEM, Hitachi S-4800). The excitation and emission spectra were recorded on a Hitachi F-4500 spectrometer equipped with a 150 W xenon lamp as the excitation source. The luminescence decay curves were obtained from a Lecroy Wave Runner 6100 Digital Oscilloscope (1 G Hz) using a tunable laser (pulse width =4 ns, gate = 50 ns) as the excitation source (Continuum Sunlite OPO). Fluorescent thermal stability of the phosphors was analyzed using a HORIBA Jobin Yvon Fluorolog-3.

## 3. Results and discussion

### 3.1 Phase analysis

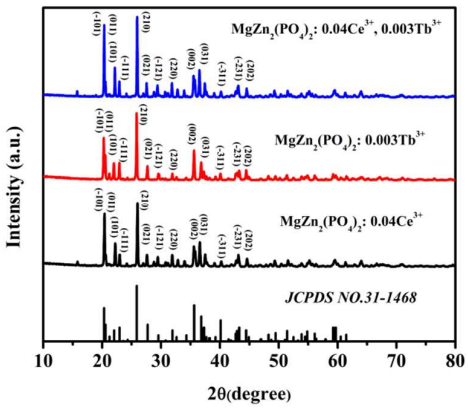


**Fig. 1** XRD patterns of $MgZn_2(PO_4)_2$: $0.04Ce^{3+}$, $MgZn_2(PO_4)_2$: $0.003Tb^{3+}$ and $MgZn_2(PO_4)_2$: $0.04Ce^{3+}$, $0.003Tb^{3+}$.

Fig. 1 shows the typical powder XRD patterns of $MgZn_2(PO_4)_2$: $0.04Ce^{3+}$, $MgZn_2(PO_4)_2$: $0.003Tb^{3+}$ and $MgZn_2(PO_4)_2$: $0.04Ce^{3+}$, $0.003Tb^{3+}$ samples. No impurity phase is observed by comparing the diffraction patterns with the standard JCPDS card (No. 31-1468). All the diffraction peaks can be indexed to the $MgZn_2(PO_4)_2$ phase with the monoclimic space group of $P2_1/c1(14)$. The uniform diffraction patterns indicate that the doped activator and sensitizer ions have almost no effect on the phase composition of $MgZn_2(PO_4)_2$.

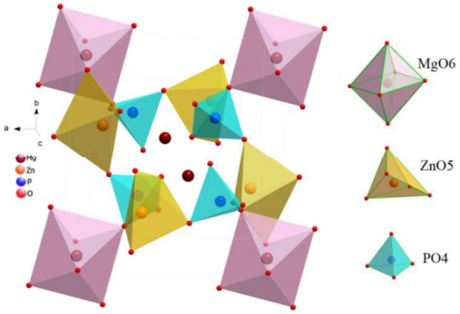


**Fig. 2** Crystal structure of $MgZn_2(PO_4)_2$ compound.

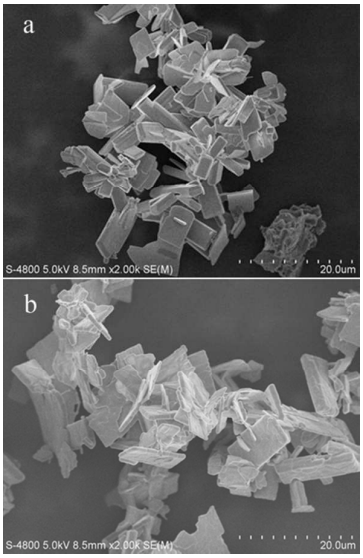


**Fig. 3** SEM images of the precursor and $MgZn_2(PO_4)_2$: $0.04Ce^{3+}$, $0.003Tb^{3+}$ obtained at 850 °C for 2 h.

The $MgZn_2(PO_4)_2$ is built up of somewhat distorted $M_{\text{I}}O_5$ trigonal bipyramids, and most regular $M_{\text{II}}O_6$ octahedra and $PO_4$ tetrahedra (Fig. 2). $MgZn_2(PO_4)_2$ with an isotypical structure of γ-$Zn_3(PO_4)_2$ is derived from α-$Zn_3(PO_4)_2$. However, there are no six-coordinated sites in the α-$Zn_3(PO_4)_2$. So it is necessary for $Mg^{2+}$ ions to enter into the six-coordinated cation sites and $Zn^{2+}$ ions in the five-coordinated sites in order to keep the ordered structure. The lattice parameters and the corresponding unit cell volumes of the prepared phosphors were calculated from the diffraction data by the Jade 6.0 program and listed in Table 1. As compared to un-doped $MgZn_2(PO_4)_2$, the unit cell constants of the Ce, Tb, Ce-Tb-doped samples slightly increase. This expansion of the lattice constants should be due to steric reasons. The ionic radii of the doped ions $Ce^{3+}$ (1.01 Å, CN=6) and $Tb^{3+}$ (0.923 Å, CN=6) are larger than those of $Zn^{2+}$ (0.68 Å, CN=5) and $Mg^{2+}$ (0.72 Å, CN=6). Base on the effective radii (r) of cations charge depending on the coordination number (CN), $Ce^{3+}$ and $Tb^{3+}$ coordination number is

the same as Mg. It can be proposed that $Ce^{3+}$ and $Tb^{3+}$ are expected to occupy the $Mg^{2+}$ sites. In this case, substitution of $Ce^{3+}$ and $Tb^{3+}$ ions could bring the positive charges in the lattices $[Ce_{Mg}]^{\cdot}$ or $[Tb_{Mg}]^{\cdot}$. The mismatch of charge on the cation sites could be balanced by the negative charges, for example, vacancy of cation: $[V_{Mg}]''$, or interstitial oxygen $[O_i]''$.

Fig. 3 is SEM images of the precursor and $MgZn_2(PO_4)_2$: $0.04Ce^{3+}$, $0.003Tb^{3+}$ sample obtained at 850°C for 2 h. From Fig. 3a, it can be seen that the precursor shows flowerlike morphology, consisting of a large number of interwoven petal-like sheets. After calcining the sheets precursor, the obtained sample is similar to the precursor in morphology and size (Fig. 3b).

**Table 1.** The calculated unit cell parameters of obtained samples.

| Sample | a (Å) | b (Å) | c (Å) | Unit cell volume (Å$^3$) |
|---|---|---|---|---|
| $MgZn_2(PO_4)_2$: $0.04Ce^{3+}$ | 7.613 | 8.383 | 5.098 | 321.350 |
| $MgZn_2(PO_4)_2$: $0.003Tb^{3+}$ | 7.572 | 8.358 | 5.067 | 319.670 |
| $MgZn_2(PO_4)_2$:$0.04Ce^{3+}$, $0.003Tb^{3+}$ | 7.758 | 8.443 | 5.107 | 320.940 |
| $MgZn_2(PO_4)_2$ | 7.569 | 8.355 | 5.059 | 318.730 |
| Space group *$P2_1/c1$(14)* | | | | |

### 3.2 Luminescence properties and energy transfer of $MgZn_2(PO_4)_2$: $Ce^{3+}$, $Tb^{3+}$ phosphor

Fig. 4 shows the excitation and emission spectra of $Ce^{3+}$ or $Tb^{3+}$ singly doped and $Ce^{3+}$-$Tb^{3+}$ co-activated $MgZn_2(PO_4)_2$ phosphors. As shown in Fig. 4a, the excitation spectrum of $MgZn_2(PO_4)_2$: $Ce^{3+}$ monitored at 324 nm exhibits a band range from 250 to 320nm, which is derived from the 4f-5d transition of $Ce^{3+}$. It can be seen that the emission spectrum consists of an asymmetric broad band with a maximum at about 324 nm under the excitation of near ultraviolet light (288nm). Usually, a double band emission is observed when $Ce^{3+}$ ions are at one specific lattice site due to the transitions from the relax lowest 5d excited state to the $^2F_{5/2}$ and $^2F_{7/2}$ spin-orbit split 4f ground states. The dependence of emission intensity on the contents of $Ce^{3+}$ for $MgZn_2(PO_4)_2$ phosphor was also shown in the inset of Fig. 4a. It can be seen that the emission intensities increase with increasing $Ce^{3+}$ concentrations, and then decrease due to the concentration quenching phenomenon. When the value of x reaches 0.04, the maximum emission intensity occurs.

The excitation and emission spectra of the $Tb^{3+}$ singly doped $MgZn_2(PO_4)_2$ sample are presented in Fig. 4b. The excitation spectrum monitored at 545nm displays several weak bands between 300 and 400 nm with a maximum at about 378 nm, which can be attributed to f-f transitions within the $4f^8$ configuration of $Tb^{3+}$. The emission spectrum under the excitation of 378 nm display a series of weak emission centered at 484 nm, 544 nm, 584 nm and 620 nm, due to the $^5D_4$-$^7F_J$ (J=6, 5, 4, and 3) characteristic transitions of $Tb^{3+}$ ions. To enhance the intensity for the $Tb^{3+}$ emission, $Ce^{3+}$ ions can be introduced as sensitizers to transfer the excitation energy to the $Tb^{3+}$ ions. It can be seen from Figure 4a and Figure 4b that there is an overlap between the emission band of $Ce^{3+}$ and the f-f absorptions band of $Tb^{3+}$. According to the formula given by Dexter [20, 21]:

$$P_{SA} = 2\pi / h\left|\langle S, A^*|H_{SA}|S^*, A\rangle\right|^2 \int_{SA} g_s(E) g_A(E) dE \quad (1)$$

where $P_{SA}$ and $H_{AS}$ are the energy transfer rate and the interaction Hamiltonian, respectively; the matrix element indicates the interaction between the initial state $|S^*, A\rangle$ and the final state $\langle S, A^*|$. The integral represents the spectral overlap between the emission spectrum of the sensitizers and the excitation spectrum of activators. From the observed spectral overlap between the emission band of $Ce^{3+}$ and the excitation of $Tb^{3+}$, it can be concluded that resonance type energy transfer may occur from $Ce^{3+}$ to $Tb^{3+}$ in $MgZn_2(PO_4)_2$ host.

This can be further confirmed by the excitation and emission spectra of $MgZn_2(PO_4)_2$: $0.04Ce^{3+}$, $0.003Tb^{3+}$in Fig. 4c. The excitation spectrum monitored at 545 nm is similar to the $MgZn_2(PO_4)_2$: $0.04Ce^{3+}$ monitored at 324 nm. The excitation spectrum shows a broad band of $Ce^{3+}$ ion which is assigned to the 4f-5d transition of $Ce^{3+}$. Under the excitation of 288 nm, the emission spectrum displays a blue band of $Ce^{3+}$ and includes a series of strong green sharp lines coming from the transitions of $Tb^{3+}$. It can be seen that the emission intensity of $MgZn_2(PO_4)_2$: $0.04Ce^{3+}$, $0.003Tb^{3+}$ at 544 nm is about 30 times as high as $MgZn_2(PO_4)_2$: $0.003Tb^{3+}$ phosphor.

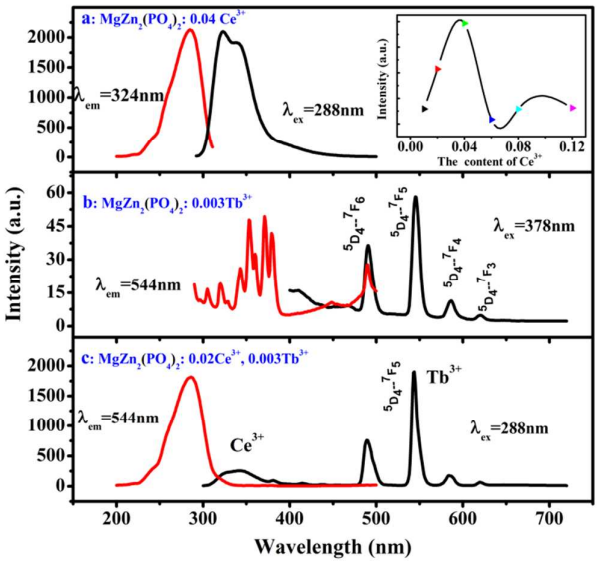


**Fig. 4** Excitation and emission spectra of phosphors: (a) $MgZn_2(PO_4)_2$: $0.04Ce^{3+}$, (b) $MgZn_2(PO_4)_2$: $0.003Tb^{3+}$, (c) $MgZn_2(PO_4)_2$: $0.04Ce^{3+}$, $0.003Tb^{3+}$, Inset in **Fig. 4a:** photoluminescence intensities of $MgZn_2(PO_4)_2$: $xCe^{3+}$ as a function of $Ce^{3+}$ contents.

In order to further investigate the energy transfer process between the $Ce^{3+}$ and $Tb^{3+}$ ions in $MgZn_2(PO_4)_2$ host lattice, a series of samples $MgZn_2(PO_4)_2$: $0.04Ce^{3+}$, $yTb^{3+}$ (y= 0, 0.003, 0.005, 0.01, 0.015, 0.02and 0.04.) were prepared, that is, the concentration of $Ce^{3+}$ was fixed at the optimal value 0.04 and the content of $Tb^{3+}$ was varied in the range of 0-0.04. Fig. 5 shows the emission spectra of $MgZn_2(PO_4)_2$: $0.04Ce^{3+}$, $yTb^{3+}$ phosphors, which were recorded at an excitation wavelength of 288 nm. It is found that the emission intensity of the $Ce^{3+}$ becomes weaker with increasing $Tb^{3+}$ concentration, whereas the emission intensities of $Tb^{3+}$ gradually strengthen and then begin to decline after reaching a maximum value at y=0.003 as a result of concentration quenching. Hence, the optimal composition of $Ce^{3+}$ and $Tb^{3+}$ co-activated phosphor is $MgZn_2(PO_4)_2$: $0.04Ce^{3+}$, $0.003Tb^{3+}$, which shows the strongest green emission. The above results indicate that the efficient energy transfer takes place from $Ce^{3+}$ to $Tb^{3+}$. Furthermore, the intensity of blue emission from $Ce^{3+}$ or the green emission from $Tb^{3+}$ could be

tuned by appropriately adjusting the relative ratio of sensitizer $Ce^{3+}$ and the activator $Tb^{3+}$.

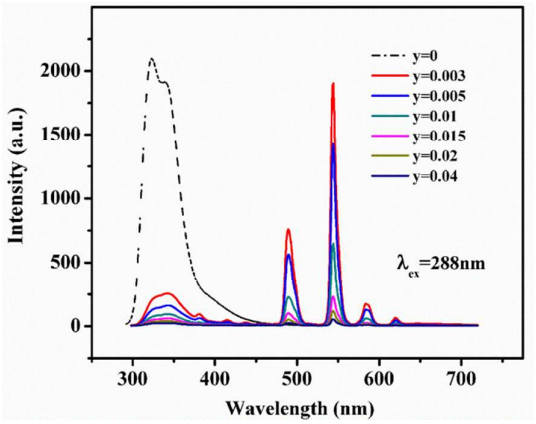


**Fig. 5** The emission spectra of $MgZn_2(PO_4)_2$: $0.04Ce^{3+}$, $yTb^{3+}$ phosphors (y= 0, 0.003, 0.005, 0.01, 0.015, 0.02, and 0.04).

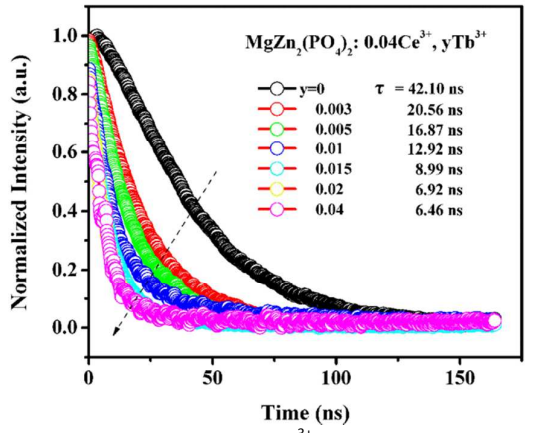


**Fig. 6** The lifetime decay curves of $Ce^{3+}$ in the $MgZn_2(PO_4)_2$: $0.04Ce^{3+}$, $yTb^{3+}$ samples.

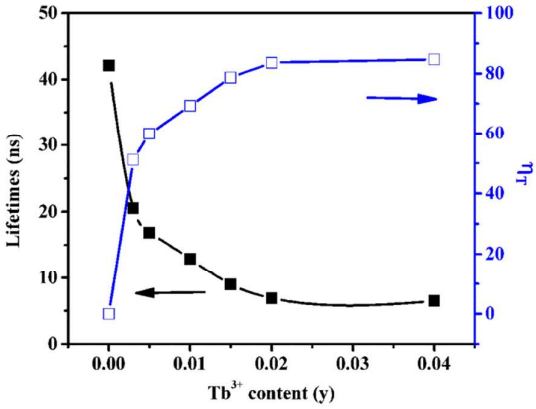


**Fig. 7** Dependence of the luminescence lifetime of $Ce^{3+}$ and energy transfer efficiency ($\eta_T$) on doped $Tb^{3+}$ ions.

The luminescence decay curves of the $Ce^{3+}$ ions in $MgZn_2(PO_4)_2$: $0.04Ce^{3+}$, $yTb^{3+}$ phosphors were measured and are shown in Fig. 6. The decay curve for $MgZn_2(PO_4)_2$: $0.04Ce^{3+}$ can be well fitted into single-exponential function, revealing that the $Ce^{3+}$ ions as the only luminescent center. This result is in agreement with the hypothesis that the $Ce^{3+}$ ion occupies the $Mg^{2+}$ ion in the host. As described by Blasse and Grabmaier [20, 21], the decay behavior of $Ce^{3+}$ can be expressed by:

$$I = I_o \exp(1-\frac{t}{\tau}) \quad (2)$$

where $I_o$ and I are the luminescence intensity at time 0 and t, respectively, and τ is the decay lifetime. For the $MgZn_2(PO_4)_2$: $0.04Ce^{3+}$, $yTb^{3+}$ (y= 0, 0.003, 0.005, 0.01, 0.015, 0.02 and 0.04) samples, the lifetime of $Ce^{3+}$ decreases with increasing $Tb^{3+}$ concentration, which are 42.10, 20.56, 16.87, 12.92, 8.99, 6.92, 6.46 ns, respectively. The energy transfer efficiency $\eta_T$ between the $Ce^{3+}$ and $Tb^{3+}$ ions was also calculated from the decay lifetime by using the equation:

$$\eta_T = 1 - \frac{\tau}{\tau_o} \quad (3)$$

where the τ and $\tau_o$ are the luminescence lifetime of the sensitizer $Ce^{3+}$ ion in presence and absence of the activator $Tb^{3+}$, respectively. The energy transfer efficiencies are plotted as a function of the $Tb^{3+}$ concentration and shown in Fig. 7. It can be seen that the lifetimes decreases monotonically while the energy transfer efficiency increase gradually with the increasing the $Tb^{3+}$ concentration. The value of $\eta_T$ reaches the maximum of 85% at y=0.04.

There are two main aspects that are responsible for the resonant energy transfer mechanism: one is the exchange interaction and the other is the multi-polar interaction. The critical distance between the sensitizer and activator should be shorter than 5 Å in the exchange interaction energy transfer[20, 21]. According to Blasse, the critical distance $R_{Ce-Tb}$ can be obtained using the following equation [21]:

$$R_{Ce-Tb} \approx 2\left[\frac{3V}{4\pi XZ}\right]^{\frac{1}{3}} \quad (4)$$

where V is the volume of the unit cell, Z is the number of formula units per unit cell, and X is the number of $Ce^{3+}$ and $Tb^{3+}$ ions. For the $MgZn_2(PO_4)_2$ host, V=328.95 $Å^3$, Z=2, and the optimal concentration of $Ce^{3+}$ and $Tb^{3+}$ are estimated to be about 0.043. According to equation (4) the critical distance $R_{Ce-Tb}$ is calculated to be 19.40 Å which is longer than 5 Å, indicating the energy transfer between $Ce^{3+}$ and $Tb^{3+}$ follows the electric multi-polar interaction mechanism.

The energy transfer is decided by the microscopic mechanism of the interaction between luminescent centers. According to the report of Van Uitert, the emission intensity per activator ion follows the below equation [24, 25]:

$$(\frac{I}{x}) = K\left[1+\beta(x)^{\frac{Q}{3}}\right]^{-1} \quad (5)$$

where x is the activator concentration, I/x is the emission intensity (I) per activator concentration (x), and K and β are constants for the same excitation condition for a given host crystal. Q=3 stands for energy transfer among the nearest neighbor ions, while Q=6, 8 or 10, indicating the electric dipole-dipole, dipole-quadrupole and quadrupole-quadrupole interactions, respectively.

The plot of lg (I/x) as a function of lg x in $MgZn_2(PO_4)_2$: $0.04Ce^{3+}$, $xTb^{3+}$ phosphors were shown in Fig. 8. It can be seen from Figure 8 that the dependence of lg (I/x) on lg (x) is linear and the slope of curve is determined to be -2.58. Then the Q is calculated approximately to be 8, implying that the dipole-quadrupole interaction is the concentration quenching mechanism of $Ce^{3+}$ and $Tb^{3+}$ doped in this phosphor.

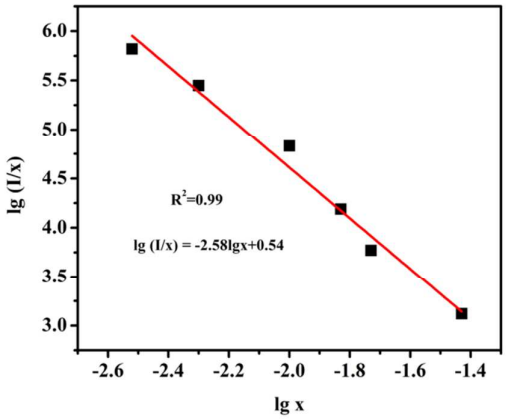


**Fig. 8** The relationship of lg (I/x)-lg (x) in $MgZn_2(PO_4)_2$: 0.04$Ce^{3+}$, y $Tb^{3+}$ phosphor.

According to Dexter's energy transfer theory, the energy transfer process through multi-polar interaction depends on the extent of overlap between the emission spectrum of the sensitizer and the absorption spectrum of the activator, the relative orientation of interacting dipoles and the distance between the sensitizer and the activator. For dipole-quadrupole interaction, the energy transfer probability $P_{SA}$ (in $s^{-1}$) from a sensitizer to an acceptor is given by the following formula 6[21]:

$$P_{Ce\text{-}Tb}^{DQ}=3.024\times10^{12}\frac{\lambda_s^2 f_q}{R_c^8\tau_s}\int\frac{f_s(E)F_A(E)}{E^4}dE \quad (6)$$

where fq is the oscillator strength of the involved absorption transition of the acceptor ($Tb^{3+}$), $\lambda_S$ (in Å) is the wavelength position of the sensitizer's emission, $\tau_S$ is the radiative decay time of the sensitizer (in seconds), R is the sensitizer-acceptor average distance (in Å), E is the energy involved in the transfer(in eV), and represents the spectral overlap between the normalized shapes of the $Ce^{3+}$ emission $f_S(E)$ and the $Tb^{3+}$ excitation $F_A(E)$. The critical distance ($R_c$) of energy transfer from the sensitizer to the acceptor is defined as the distance for which the probability of transfer equals the probability of radiative emission of donor, the distance for which $P^{DQ}\tau_S = 1$. Hence, $R_c$ can be obtained from eq (7) as

$$R_c^8=3.024\times10^{12}\lambda_s^2 f_q\int\frac{f_s(E)F_A(E)}{E^4}dE \quad (7)$$

However, the oscillator strength of the $Tb^{3+}$ quadrupole transitions ($f_q$) was not obtained up to now. It is suggested by Verstegen *et al.* that the ratio $f_q/f_d$ is about $10^{-3}$ to $10^{-2}$, where $f_d = 10^{-6}$ is the oscillator strength of the $Tb^{3+}$ electric dipole transition. Using $\lambda_s$ =3240 Å, $f_q = 10^{-3}$-$10^{-2}f_d$, the critical distance ($R_c$) for the dipole-quadrupole interaction method is 15.45-20.59 Å. This result is in good agreement with above obtained results using the concentration quenching method (19.40 Å), which confirms that the mechanism of energy transfer from $Ce^{3+}$ to $Tb^{3+}$ ions is mainly due to a dipole-quadrupole interaction.

On the basis of above mentioned spectra analysis, the energy level scheme with the electronic transitions of $Ce^{3+}$, $Tb^{3+}$ and energy transfer processes of $Ce^{3+}$ and $Tb^{3+}$ is schematically shown in Fig. 9. When the $Ce^{3+}$ ions irradiated by UV light, an electron is excited to the high 5d level; One part of the absorption energy of $Ce^{3+}$ has been released in the form of broad-band emission of 324 nm and 341 nm light and the other part is transferred to the $Tb^{3+}$. An energy transfer process occurs from the excited 5d state of $Ce^{3+}$ ($^2D_{3/2}$) to the $^5D_3$ level of $Tb^{3+}$, which is ascribed to the similar value of the energy level, and gives the lower vibration frequency of phonon emission. Finally, the excited $Tb^{3+}$ relaxes to the $^5D_4$ non-radioactively level and shows the strong emission of $Tb^{3+}$ ($^5D_4$-$^7F_J$, J= 3, 4, 5 and 6).

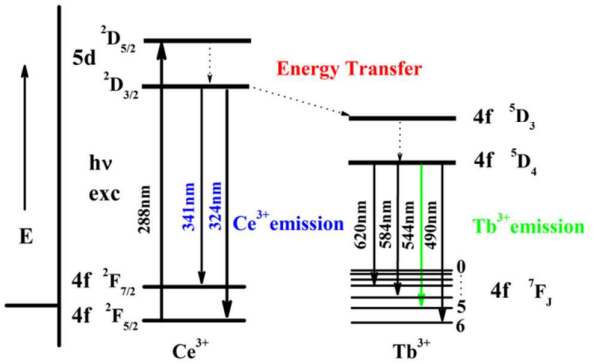


**Fig. 9** The luminescence and energy transfer process of $Ce^{3+}$ and $Tb^{3+}$ in $MgZn_2(PO_4)_2$: $Ce^{3+}$, $Tb^{3+}$ phosphors.

### 3.3 Thermal stability and CIE coordinates

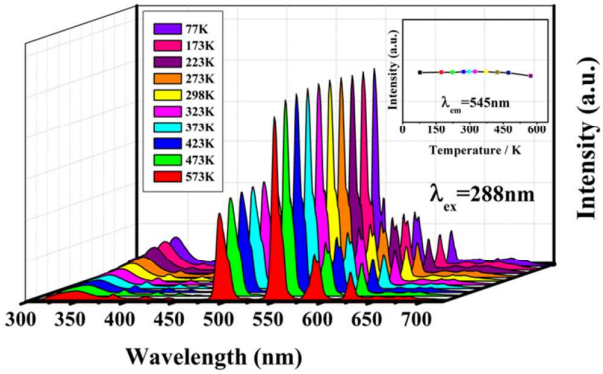


**Fig. 10** Emission spectra of $MgZn_2(PO_4)_2$: 0.04$Ce^{3+}$, 0.003$Tb^{3+}$ phosphor at a temperatures range from 77K to 573K under the excitation of 288 nm.

Thermal stability of the phosphor has a considerable influence on the light output and color rendering index. Generally, the phosphor of the LEDs are required to sustain their conversion efficiency up to 423K due to the fact that the temperature of an LED package rises by the heat generation from the LED itself during the LED operation. The reason for this has been reported as an increase in the non-radiative transition probability in the configurational coordinated diagram. The temperature dependence of the luminescence of $MgZn_2(PO_4)_2$: 0.04$Ce^{3+}$, 0.003$Tb^{3+}$ under 288 nm excitation is shown in Fig. 10. Upon heating the phosphor samples in the temperature range from 77K to 573K, the emission intensity decreased slightly, since the probability of nonradiation is increased and luminescent c enter is released through the crossing point between the excitation state and the ground state, causing the luminescence quenching. In addition, the emission wavelengths show no shifts with increasing temperature. The emission intensities of $MgZn_2(PO_4)_2$: 0.04$Ce^{3+}$, 0.003$Tb^{3+}$ maintains 88% of the initial emission intensity corresponding to a temperature of 423K.

Furthermore, to further verify the origin of temperature dependent emission intensity ($I_T$), the activation energy (ΔE) was calculated using the Arrhenius equation [26]:

$$I_T = I_o / \left[1 + c\exp(-\frac{\Delta E}{kT})\right] \quad (8)$$

where $I_o$ is the initial emission intensity of the phosphor at room temperature, $I_T$ is the emission intensity at different temperatures, c is a constant, ΔE is the activation energy for thermal quenching, and k is Boltzmann constant (k=8.62 * $10^{-5}$ eV). According to the equation, the activation energy ΔE can be calculated from a plotting of $\ln[I_o/I_T-1]$ against 1/kT, where the slope of the straight line equals -ΔE. As shown in Fig. 11, ΔE was found to be 0.311 eV for $Tb^{3+}$. The relatively high activation energy results in a good thermal stability for this phosphor. Hence, the phosphor shows an excellent thermal stability and outstanding luminescence properties, indicating that the $MgZn_2(PO_4)_2$: $Ce^{3+}$, $Tb^{3+}$ phosphor has promising application in light emitting field.

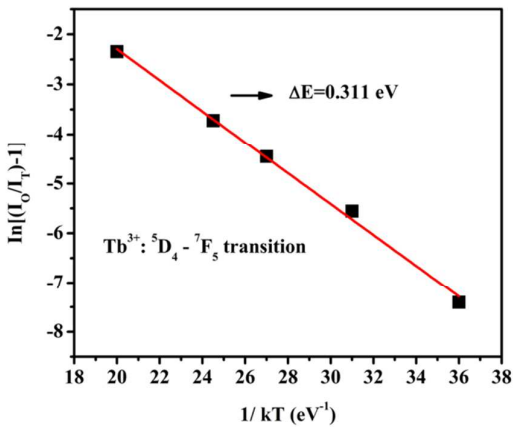


**Fig. 11** A $\ln[I_O/I_T-1]$ - 1/kT activation energy graph for thermal quenching of $Tb^{3+}$ in $MgZn_2(PO_4)_2$: $0.04Ce^{3+}$, $0.003Tb^{3+}$ phosphor.

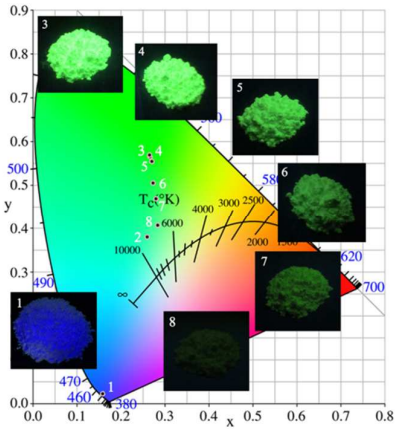


**Fig. 12** CIE chromaticity diagram for $MgZn_2(PO_4)_2$: $xCe^{3+}$, $yTb^{3+}$ phosphors: (1) x=0.04, y=0; (2) x=0, y=0.003; (3) x=0.04, y=0.003; (4) x=0.04, y=0.005; (5) x=0.04, y=0.01; (6) x=0.04, y=0.015; (7) x=0.04, y=0.02; (8) x=0.04, y=0.04; The inset photographs show the samples excited under a 254 nm lamp irradiation.

The chromaticity diagram is a tool to specify how the human eyes will experience light with a given spectrum, which could intuitively illuminate the changes of the emission color of the phosphor. The x and y values of the CIE chromaticity coordinates of the $MgZn_2(PO_4)_2$: $xCe^{3+}$, $yTb^{3+}$ phosphors with different dopant contents were measured based on their emission spectra and presented in Fig. 12. The CIE chromaticity coordinates of the $Ce^{3+}$ and $Tb^{3+}$ single doped phosphors are (0.1588, 0.0220) and (0.2600, 0.3797), corresponding to dark blue and cyan light, respectively. In $MgZn_2(PO_4)_2$: $0.04Ce^{3+}$, $yTb^{3+}$ samples, as y increased from 0 to 0.015, the CIE coordinates shifted from (0.1588, 0.0220) to (0.2659, 0.5691), the emitting color was changed from blue to green (Tab 2). Thus, the emission of the phosphor can be tuned by adjusting the doping content of $Tb^{3+}$ ions. The inset pictures in Fig. 12 show the luminescence image of blue-emitting $MgZn_2(PO_4)_2$: $0.04Ce^{3+}$ and green-emitting $MgZn_2(PO_4)_2$: $0.04Ce^{3+}$, $yTb^{3+}$ phosphors with 254 nm excitation.

**Table 2** The CIE chromaticity coordinates of $MgZn_2(PO_4)_2$: $xCe^{3+}$, $yTb^{3+}$ (x=0, 0.04, y=0, 0.003, 0.005, 0.01, 0.015, 0.02,0.04) under 288 nm UV excitation.

| Point | Sample （λex=288 nm） | CIE (x, y) |
|---|---|---|
| 1 | $MgZn_2(PO_4)_2$: 0.04 $Ce^{3+}$ | (0.1588, 0.0220) |
| 2 | $MgZn_2(PO_4)_2$: 0.003 $Tb^{3+}$ （$\lambda_{ex}$=378 nm） | (0.2600, 0.3797) |
| 3 | $MgZn_2(PO_4)_2$: 0.04 $Ce^{3+}$, 0.003 $Tb^{3+}$ | (0.2671, 0.5654) |
| 4 | $MgZn_2(PO_4)_2$: 0.04 $Ce^{3+}$, 0.005 $Tb^{3+}$ | (0.2659, 0.5691) |
| 5 | $MgZn_2(PO_4)_2$: 0.04 $Ce^{3+}$, 0.01 $Tb^{3+}$ | (0.2709, 0.5552) |
| 6 | $MgZn_2(PO_4)_2$: 0.04 $Ce^{3+}$, 0.015 $Tb^{3+}$ | (0.2727, 0.5052) |
| 7 | $MgZn_2(PO_4)_2$: 0.04 $Ce^{3+}$, 0.02 $Tb^{3+}$ | (0.2799, 0.4694) |
| 8 | $MgZn_2(PO_4)_2$: 0.04 $Ce^{3+}$, 0.04 $Tb^{3+}$ | (0.2844, 0.4071) |

## Conclusions

In summary, a novel green phosphor $MgZn_2(PO_4)_2$: $0.04Ce^{3+}$, $0.003Tb^{3+}$ was obtained via co-precipitation method followed by calcination at 850 °C for 2 h in 5%$N_2$-95%$H_2$ atmosphere. An efficient energy transfer from $Ce^{3+}$ to $Tb^{3+}$ through a non-radiative process in the co-doped samples was observed, which results in enhanced green emission of $Tb^{3+}$ at 544 nm. The energy transfer from $Ce^{3+}$ to $Tb^{3+}$ has been demonstrated to be the electric dipole-quadrupole interaction, and the energy transfer efficiency is over 85%. The energy transfer critical distance was calculated to be 19.40 Å. The novel phosphors have excellent thermal stability and luminescence properties, and thus are very promising as green emitting phosphor in lighting field.

## Acknowledgements

This work was financially supported by the National Science Foundation of China (21266030), the Achievement Transformation Project of Xinjiang province (201154141), the Technological Innovation Youth Training Project of Xinjiang Autonomous (2013731006), and the Research Fund for the Doctoral Program of Higher Education of China (20126501120003).

## Notes and references

1 Z. Y. Hou, G. G. Li, H. Z. Lian, and J. Lin, *J. Mater. Chem.*, 2012, 22, 5254.
2 C. Feldmann, T. Jüstel, C. R. Ronda, and P. J. Schmidt, *Adv. Funct. Mater.*, 2003, 13, 511.
3 Y. C. Jia, W. Lu, N. Guo, W. Z. Lu, Q. Zhao, and H. P. You, *Phys. Chem. Chem. Phys.*, 2013, 15, 13810.
4 W. Lu, N. Guo, Y. C. You, Q. Zhao, W. Z. Lv, M. M. Jiao, B. Q. Shao, and H. P. You, *Inorg. Chem.*, 2013, 52, 3007.

5 D. L. Geng, M. M. Shang, D. M. Yang, Y. Zhang, Z. Y. Cheng, and J. Lin, *Dalton. Trans.*, 2012, 41, 14042.
6 A. Nohara, S. Takeshita, and T. Isobe, *RSC. Adv.*, 2014, 4, 11219.
7 X. Y. Fu, L. J. Fang, S. Y. Niu, and H. W. Zhang, *J. Lumin.*, 2013, 142, 163.
8 Z. F. Yang, Y. H. Hu, L. Chen, X. J. Wang, and G. F. Ju, *Mater. Sci. Eng. B.*, 2015, 193, 27.
9 Z. G. Xia, Y. J. Liang, D. Y. Yu, M. F. Zhang, W. Z. Huang, M. H. Tong, J. M. Wu, and J. W. Zhao, *Opt. & Laser. Tech.*, 2014, 56, 387.
10 H. H. Lin, G. B. Zhang, P. A. Tanner, and H. B. Liang, *J. Phys. Chem. C.*, 2013, 117, 12769.
11 J. Y. Sun, G. C. Sun, and Y. N. Sun, *Ceram. Int.*, 2014, 40, 1723.
12 N. L. Wang, S. Z. Zhang, X. Y. Zhang, and Y. Wei, *Ceram. Int.*, 2014, 40, 16253.
13 G. H. Li, S. Lan, L. L. Li, M. M. Li, W. W. Bao, H. F. Zou, X. C. Xu, and S. C. Gan, *J. Alloys. Compd.*, 2012, 513, 145.
**14** A. G. Nord, *Mater. Res. Bull.*, 1977, 12, 563.
15 A. G. Nord, *Mater. Res. Bull.*, 1982, 17, 1001.
16 A. G. Nord, and T. Stefanidis, *Mater. Res. Bull.*, 1980, 15, 1183.
17 Nord, A. G.; Stefanidis, T. Crystal chemistry of γ-(Zn, Me)$_3$(PO$_4$)$_2$ solid solutions. *Mater. Res. Bull.* 1981, 16, 1121.
18 A. G. Nord, and T. Stefanidis, *Polyhedron*., 1982, 1, 349.
19 C. Calvo, *J. Phys. Chem. Solids.*, 1963, 24,141.
20 D. L. Dexter, *J. Chem. phys.*, 1953, 21, 836.
21 G. Blasse, *Philips. Res. Rep.*, 1969, 24, 131.
22 K. Li, Y. Zhang, X. J. Li, M. M. Shang, H. Z. Lian, and J. Lin, *Dalton. Trans.*, 2015, 44, 4683.
23 P. I. Paulose, G. Jose, V. Thomas, N. V. Unnikrishnan, and K. R. M. Warrier, *J. Phys. Chem. Solids.*, 2003, 64, 841.
24 L. Ozawa, and P. M. Jaffe, *J. Electrochem. Soc.*, 1971, 118, 1678.
25 L. G. Van Uitert, *J. Electrochem. Soc.*, 1967, 114, 1048.
26 J. Zhou, and Z. G. Xia, *J. Mater. Chem. C.*, 2014, 2, 6978.